

---

This is an electronic reprint of the original article.  
This reprint may differ from the original in pagination and typographic detail.

Author(s): Laurson, Lasse & Alava, Mikko J.  
Title: Dynamic Hysteresis in Cyclic Deformation of Crystalline Solids  
Year: 2012  
Version: Final published version

**Please cite the original version:**

Laurson, Lasse & Alava, Mikko J. 2012. Dynamic Hysteresis in Cyclic Deformation of Crystalline Solids. *Physical Review Letters*. Volume 109, Issue 15. 155504/1-5. ISSN 0031-9007 (printed). DOI: 10.1103/physrevlett.109.155504.

Rights: © 2012 American Physical Society (APS). This is the accepted version of the following article: Laurson, Lasse & Alava, Mikko J. 2012. Dynamic Hysteresis in Cyclic Deformation of Crystalline Solids. *Physical Review Letters*. Volume 109, Issue 15. 155504/1-5. ISSN 0031-9007 (printed). DOI: 10.1103/physrevlett.109.155504, which has been published in final form at <http://journals.aps.org/prl/abstract/10.1103/PhysRevLett.109.155504>.

---

All material supplied via Aaltodoc is protected by copyright and other intellectual property rights, and duplication or sale of all or part of any of the repository collections is not permitted, except that material may be duplicated by you for your research use or educational purposes in electronic or print form. You must obtain permission for any other use. Electronic or print copies may not be offered, whether for sale or otherwise to anyone who is not an authorised user.

## Dynamic Hysteresis in Cyclic Deformation of Crystalline Solids

Lasse Laurson and Mikko J. Alava

*COMP Centre of Excellence, Department of Applied Physics, Aalto University, PO Box 14100, 00076 Aalto, Espoo, Finland*  
(Received 10 May 2012; revised manuscript received 12 June 2012; published 12 October 2012)

The hysteresis or internal friction in the deformation of crystalline solids stressed cyclically is studied from the viewpoint of collective dislocation dynamics. Stress-controlled simulations of a dislocation dynamics model at various loading frequencies and amplitudes are performed to study the stress–strain rate hysteresis. The hysteresis loop areas exhibit a maximum at a characteristic frequency and a power law frequency dependence in the low frequency limit, with the power law exponent exhibiting two regimes, corresponding to the jammed and the yielding or moving phases of the system, respectively. The first of these phases of the system exhibits nontrivial critical-like viscoelastic dynamics, crossing over to intermittent viscoplastic deformation for higher stress amplitudes.

DOI: [10.1103/PhysRevLett.109.155504](https://doi.org/10.1103/PhysRevLett.109.155504)

PACS numbers: 61.72.Lk, 62.40.+i, 68.35.Rh

The response of interacting many-body systems to oscillating external fields is an old problem in physics, with many applications in materials science and engineering. In general, due to the competing time scales of the internal relaxation and the external perturbation the response will generally be out of phase with respect to the external field [1]. This gives rise to a dynamic hysteresis loop with an area depending on the driving frequency and amplitude. In a magnet driven by an oscillating magnetic field  $h(t)$ , the magnetization  $m(t)$  lagging behind the field leads to a nonvanishing hysteresis loop area  $A = \oint mdh$  [2]. Hysteresis as such is a very general phenomenon, and has been studied in many contexts from the mechanical response of materials [3], to electronics [4], cell biology [5], neurobiology [6], and quantum systems [7].

Mechanical dissipation or internal friction is one manifestation of the dynamics of dislocations in crystalline solids. Stress-strain hysteresis, in stress or strain controlled experiments [3], is related via the hysteresis loop area to the energy dissipated per cycle. Since dislocations are linelike objects, internal friction has also been described microscopically by the back-and-forth dissipative motion of individual dislocation segments [8]. However, plastic, irreversible deformation has been shown over the last decade to be a highly cooperative process with avalanche dynamics and long-range spatiotemporal correlations [9]. Even the simplest dislocation dynamics models—which nevertheless describe to a large degree some real materials—demonstrate phenomena like a yielding or jamming transition at a critical applied stress  $\sigma = \sigma_c$  separating a phase with frozen dislocations from a moving phase with a stress-dependent average strain rate—the order parameter of the transition [10–12]. This is in analogy to systems exhibiting criticality due to a depinning transition—separating in the adiabatic, thermodynamic limit frozen and active states, with the order parameter given by the average velocity—such as interfaces in random media [13] and vortices in type-II superconductors [14].

In this Letter we consider the dynamic strain rate hysteresis of dislocation assemblies from the viewpoint of collective dislocation dynamics. The important aspects are (i) the various behaviors in the phase diagram, characterized by the amplitude and the frequency of the external driving, (ii) the collective phenomena that underlie the observations from the simulations, and (iii) the theoretical and experimental implications of our results. We discuss the scaling of the hysteresis, and link it to a picture related to depinning transitions. Recent theoretical ideas suggest that due to the long-range dislocation stress fields this transition should be described by the mean field depinning transition [15,16]. However, our results suggest that this simple picture is incomplete, calling for novel theoretical ideas to properly describe the glassy, critical-like dynamics observed in the jammed phase of the system.

Dislocation physics has been recently studied with many simplified models from discrete dislocation dynamics [17–19] to phase field [20] and automaton models [21]. Here, we consider the stress-controlled hysteretic dynamics within a two-dimensional discrete dislocations dynamics model [17]. Such a model captures many of the interesting aspects of real crystal plasticity, including the scale free distribution of avalanches of plastic deformation [22], as well as an Andrade primary creep law [10–12]. It represents a cross section ( $xy$  plane) of a single crystal with a single slip geometry and straight parallel edge dislocations along the  $z$  axis. The  $N$  dislocations glide along directions parallel to their Burgers vectors  $\vec{b} = \pm b\vec{u}_x$ . Equal numbers of dislocations with positive and negative Burgers vectors are assumed, and dislocation climb is not considered for simplicity. The dislocations interact through their long-range stress fields,  $\sigma_s(\vec{r}) = Dbx(x^2 - y^2)/(x^2 + y^2)^2$ , where  $D = \mu/2\pi(1 - \nu)$ , with  $\mu$  the shear modulus and  $\nu$  the Poisson ratio of the material. The overdamped equations of motion read  $\chi_d^{-1}v_n/b = s_n b[\sum_{m \neq n} s_m \sigma_s(\vec{r}_{nm}) + \sigma(t)]$ , with  $v_n$  the velocity and  $s_n$

the sign of the  $n$ th dislocation;  $\chi_d$  is the dislocation mobility, implicitly including effects due to thermal fluctuations, and  $\sigma(t)$  is the sinusoidal external stress,  $\sigma(t) = \sigma_0 \sin(\omega t)$ , with  $\sigma_0$  the amplitude and  $\omega$  the angular frequency. The equations of motion are integrated with an adaptive step size fifth order Runge-Kutta algorithm, by measuring lengths in units of  $b$ , times in units of  $1/(\chi_d D b)$ , and stresses in units of  $D$ , and by imposing periodic boundary conditions in both the  $x$  and  $y$  directions. Two dislocations of opposite sign with a mutual distance smaller than  $2b$  are removed from the system (dislocation annihilation).

The simulations are started from a random initial configuration of  $N_0 = 1600$  dislocations within a square cell of linear size  $L = 200b$ . The system first relaxes with  $\sigma(t) = 0$ , to a metastable dislocation arrangement. After the annihilations during the relaxation,  $N = 500\text{--}600$  dislocations remain. Then, the oscillating external stress is turned on, and the evolution of the system is monitored by measuring the time dependence of the strain rate,  $d\epsilon(t)/dt \equiv \epsilon_t(t) = b/L^2 \sum_n s_n v_n(t)$ . We simulate the system extensively for a wide range of  $\sigma_0$  and  $\omega$  values, with several realizations of the random initial configuration considered in each case.

The resulting stress–strain rate hysteresis loops exhibit a variety of properties, depending on  $\sigma_0$  and  $\omega$ . After an initial transient, the system tends to settle into a “locked-in” steady state (usually reached within the 20 cycles we consider) in which the same hysteresis loop is repeated with a clockwise rotation direction in the  $\sigma$ – $\epsilon_t$  plane. Figure 1 shows examples of such locked-in loops for different  $\sigma_0$  and  $\omega$ . For small  $\sigma_0$  and large  $\omega$  (i.e., under conditions where a typical distance traveled per cycle by a dislocation is small), the loops are smooth and the strain rate  $\epsilon_t(t)$  obeys sinusoidal dynamics with a well-defined phase difference compared to the external drive. During the initial transient leading to this smooth steady state, the system typically exhibits bursty dislocation rearrangements, but will settle into a smooth locked-in state after a few cycles. For larger  $\sigma_0$  and/or smaller  $\omega$ , even the steady state cyclic dislocation dynamics becomes intermittent, characterized by avalanchelike dislocation rearrangements. Interestingly, also in this case the system is usually able to find a locked-in steady state within the 20 cycles we consider, repeating the same bursty dynamics during each cycle in the steady regime. The transient time to reach the steady state tends to increase upon increasing  $\sigma_0$  and decreasing  $\omega$ . For large  $\sigma_0$  and low  $\omega$  (bottom right corner of Fig. 1), the loops exhibit curvature consistent with the idea that the low-frequency limit is described by  $\epsilon_t \sim (\sigma - \sigma_c)^\beta$ , with  $\beta > 1$  [10].

We proceed to characterize the intermittency of the steady state cyclic dislocation dynamics, by considering the average normalized absolute deviations of  $\epsilon_t(t)$  from a best-fit sinusoidal function,

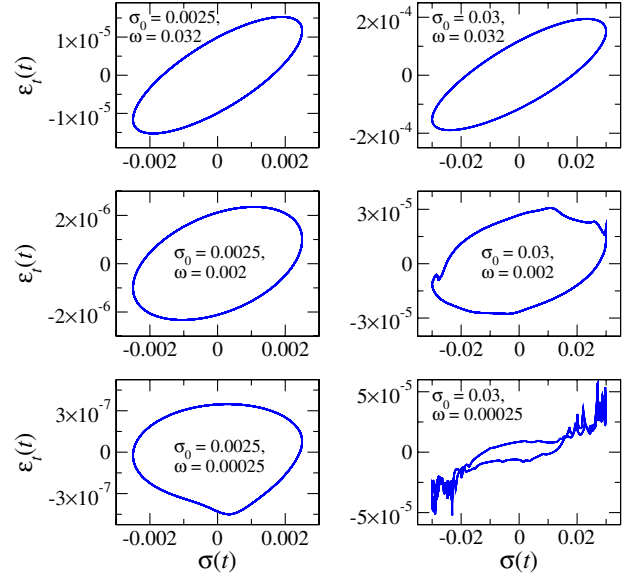


FIG. 1 (color online). Examples of typical “locked-in” strain rate hysteresis loops reached by the system after a transient, for low and high stress amplitude (left and right column, respectively) and for various frequencies. All loops exhibit a clockwise rotation direction. For small  $\sigma_0$  and/or large  $\omega$  the loops are smooth, but become increasingly intermittent with increasing  $\sigma_0$  and decreasing  $\omega$ . Notice that due to the large variation of  $\epsilon_t$  values for the different parameter values considered, the  $\epsilon_t$  axis scales are different in different subfigures.

$$\Delta \epsilon_t = \langle |\epsilon_t(t) - \epsilon_{t,0} \sin(\omega t + \omega_0)| \rangle / \epsilon_{t,0}, \quad (1)$$

where  $\epsilon_{t,0}$  and  $\omega_0$  are fitting parameters, and  $\langle \dots \rangle$  indicates an average over both time and different initial configurations. Large values of  $\Delta \epsilon_t$  indicate the presence of non-trivial or intermittent dynamics. Figure 2 shows  $\Delta \epsilon_t$  as a function of  $\sigma_0$  for various  $\omega$ , demonstrating that the intermittency increases with  $\sigma_0$  and decreases with  $\omega$ . By applying a threshold value for  $\Delta \epsilon_t$ , one finds a phase boundary separating “phases” with smooth and intermittent dynamics in the  $\sigma_0$ – $\omega$  plane (inset of Fig. 2). The precise location of this boundary depends on the threshold value used, but qualitatively the phase diagram looks the same for a range of threshold values.

Our main result concerns the area  $A_{\text{hyst}}(\sigma_0, \omega) = \oint \epsilon_t d\sigma$  of the steady state stress–strain rate hysteresis loops as a function of  $\sigma_0$  and  $\omega$ . These are summarized in Fig. 3.  $A_{\text{hyst}}(\sigma_0, \omega)$  exhibits a maximum at a characteristic frequency  $\omega^* \approx 0.06$  independent of  $\sigma_0$ , corresponding to the resonance frequency of the effective confining potential (see the oscillator model below). The  $A_{\text{hyst}}(\omega)$  data for various  $\sigma_0$  can be collapsed by normalizing with  $\sigma_0^2$ , leading to two distinct low frequency power laws  $A_{\text{hyst}} \sim \omega^\kappa$ , with exponents  $\kappa \approx 0.82$  and  $\kappa \approx 0.69$  for  $\sigma_0 < 0.015$  and  $\sigma_0 > 0.015$ , respectively. The stress amplitude value  $\sigma_0 = \sigma_c \approx 0.015$  separating these two regimes corresponds roughly to the maximum  $\sigma$  value

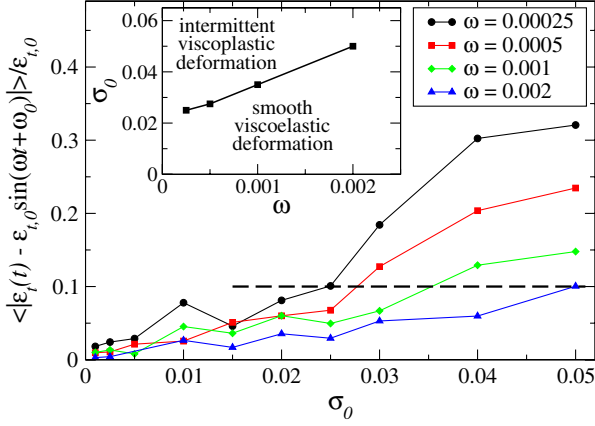


FIG. 2 (color online). Normalized absolute deviations of  $\dot{\epsilon}_t(t)$  from a best-fit sinusoidal function,  $\dot{\epsilon}_{t,0} \sin(\omega t + \omega_0)$ , characterizing the intermittency of the cyclic dislocation dynamics in the “locked-in” steady state as a function of  $\sigma_0$ , for various  $\omega$ . The inset shows a phase diagram in the  $\omega - \sigma_0$  space, displaying smooth and intermittent phases separated by a phase boundary obtained by thresholding the data in the main figure, with the threshold shown as a dashed line.

for which the power-law Andrade creep is observed in a constant stress simulation, i.e.,  $\epsilon_t \sim t^{-\theta}$  with  $\theta$  close to  $2/3$  [10,11,23–25]. For a larger applied stress in the dc-driven case, the system would reach a (quasi)stationary moving or flowing state with a nonzero mean strain rate [10]. Thus, we argue that the two stress amplitude regimes with the different  $\kappa$  values correspond to the jammed [ $\sigma_0 < \sigma_c(N)$ ] and moving [ $\sigma_0 > \sigma_c(N)$ ] states of the system for a constant external stress, respectively.

We note that the magnitude of  $A_{\text{hyst}}$  is related to both the phase difference between  $\sigma(t)$  and  $\dot{\epsilon}_t(t)$ , and to the strain rate amplitude, i.e.,  $\omega_0$  and  $\dot{\epsilon}_{t,0}$  in Eq. (1). Figure 4 shows

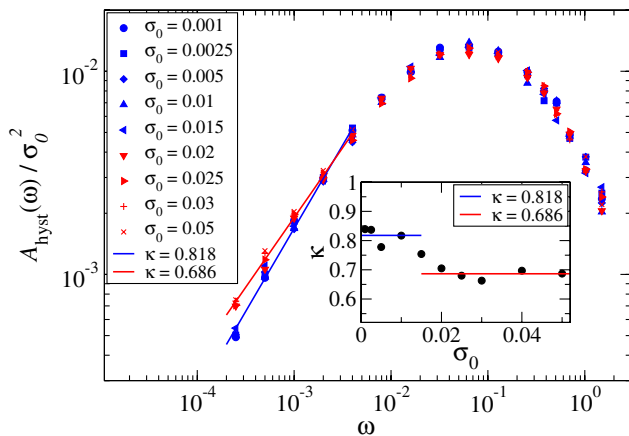


FIG. 3 (color online). The scaled hysteresis loop areas  $A_{\text{hyst}}/\sigma_0^2$  for various  $\sigma_0$  as a function of  $\omega$ , showing a data collapse with two distinct low-frequency power laws,  $A_{\text{hyst}} \sim \omega^\kappa$ , with  $\kappa \approx 0.82$  for  $\sigma_0 < 0.015 \approx \sigma_c$  and  $\kappa \approx 0.69$  for  $\sigma_0 > 0.015$ . The inset shows the measured  $\kappa$  as a function of  $\sigma_0$ .

that for  $\sigma_0 < \sigma_c$ ,  $\omega_0$  is independent of  $\sigma_0$  and approaches  $\pi/2$  for  $\omega \rightarrow 0$ , and goes to zero for large  $\omega$ . Viscoelasticity is typically characterized by the phase lag  $\delta$  between  $\sigma(t) = \sigma_0 \sin(\omega t + \delta)$  and  $\epsilon(t) = \epsilon_0 \sin(\omega t)$ , with  $\delta = 0$  and  $\pi/2$  corresponding to perfectly elastic and viscous dynamics, respectively. Thus, the relation  $\omega_0 = \pi/2 - \delta$  implies that the dynamics extrapolates between perfect elasticity for  $\omega \rightarrow 0$  and perfectly viscous dynamics in the high-frequency limit. For  $\sigma_0 > \sigma_c$ ,  $\omega_0$  starts to decrease for small  $\omega$ , indicating the presence of plastic dislocation rearrangements, also visible in the intermittency of the dynamics (Fig. 2). Rescaling the strain rate amplitude by  $\sigma_0$  leads to a data collapse for  $\sigma_0 < \sigma_c$ , with  $\dot{\epsilon}_{t,0}/\sigma_0 \sim \omega^\kappa$ ,  $\kappa \approx 0.82$  for small  $\omega$ , while for large  $\omega$ ,  $\dot{\epsilon}_{t,0}/\sigma_0 \rightarrow Nb/L^2 \approx 0.0125$ , corresponding to  $N \approx 500$  dislocations freely following  $\sigma(t)$  in a system of size  $L = 200b$ . For  $\sigma_0 > \sigma_c$ , there are deviations from the low-frequency power law, again corresponding to intermittent viscoplastic deformation.

As a naive attempt to understand the observed scaling behavior, we consider a simple oscillator model for the dislocation dynamics. In general, dislocations will oscillate back and forth due to the sinusoidal applied stress. However, dislocation interactions induce a tendency to form dislocation structures of varying complexity—dislocation multipoles—with each multipole moving together with a strain rate  $\dot{\epsilon}_t^{(i)}$  in a way dictated by its net Burgers vector  $b^{(i)}$  under the applied field and interactions with the rest of the system. For small  $\sigma_0$  and large  $\omega$  we describe the latter by a harmonic potential, and write the equation of motion for the  $i$ th multipole as

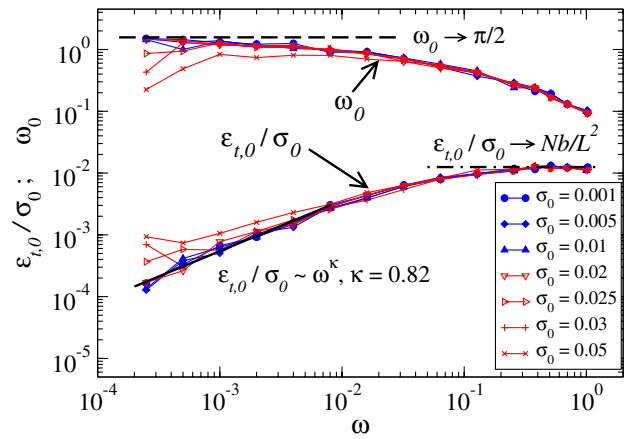


FIG. 4 (color online). The phase difference  $\omega_0$  (upper curves) and the scaled strain rate amplitude  $\dot{\epsilon}_{t,0}/\sigma_0$  (lower curves) for various  $\sigma_0$ . For  $\sigma_0 < \sigma_c$ ,  $\omega_0$  approaches  $\pi/2$  for  $\omega \rightarrow 0$  (dashed line, a signature of perfectly elastic dynamics), while for larger  $\sigma_0$ ,  $\omega_0$  starts to decrease for small  $\omega$ , indicating the presence of plastic rearrangements.  $\dot{\epsilon}_{t,0}/\sigma_0$  obeys a power law  $\dot{\epsilon}_{t,0}/\sigma_0 \sim \omega^\kappa$  for  $\sigma_0 < \sigma_c$  (solid line, with deviations from the power law for  $\sigma_0 > \sigma_c$ ), and approaches a value  $\dot{\epsilon}_{t,0}/\sigma_0 = Nb/L^2 \approx 0.0125$  (dash-dotted line) for large  $\omega$ .

$$\frac{L^2 \epsilon_t^{(i)}(t)}{b_i} \equiv x_t^{(i)}(t) = -K^{(i)}[x^{(i)}(t) - x^{(i)}(0)] + \sigma_0 \sin(\omega t), \quad (2)$$

where  $K^{(i)}$  is the effective spring constant characterizing the confining potential of the  $i$ th multipole [with a center of mass  $x^{(i)}(t)$ ] due to long-range interactions with the other multipoles. The asymptotic ( $t \rightarrow \infty$ ) solution of Eq. (2) is given by

$$\epsilon_t^{(i)}(t) = \frac{b^{(i)} \sigma_0}{L^2} \frac{[K^{(i)} \omega \cos(\omega t) + \omega^2 \sin(\omega t)]}{(K^{(i)})^2 + \omega^2}. \quad (3)$$

The total strain rate is obtained by summing over the multipoles,  $\epsilon_t = \sum_i \epsilon_t^{(i)}$ . Disregarding fluctuations by setting  $b^{(i)} = b_{\text{eff}}$  and  $K^{(i)} = K_{\text{eff}}$  for all  $i$ , one obtains

$$\epsilon_t(t) = \frac{b_{\text{eff}} N_{\text{mp}} \sigma_0}{L^2} \frac{K_{\text{eff}} \omega \cos(\omega t) + \omega^2 \sin(\omega t)}{K_{\text{eff}}^2 + \omega^2}, \quad (4)$$

with  $N_{\text{mp}}$  the number of dislocation multipoles in the system. Notice that Eq. (4) corresponds to a clockwise direction of rotation in the  $\sigma$ - $\epsilon_t$  plane, as observed in the simulations. The area of the hysteresis loop,  $A_{\text{hyst}} = \oint \epsilon_t d\sigma$ , is given by

$$A_{\text{hyst}}(\omega, \sigma_0) = \frac{b_{\text{eff}} N_{\text{mp}} \sigma_0^2}{L^2} \frac{\pi K_{\text{eff}} \omega}{K_{\text{eff}}^2 + \omega^2}. \quad (5)$$

Equation (5) predicts a maximum of  $A_{\text{hyst}}$  around  $\omega = \omega^* \approx K_{\text{eff}}$ , and a power law frequency dependence  $A_{\text{hyst}} \sim \omega^{-1}$  and  $A_{\text{hyst}} \sim \omega^1$  for  $\omega \gg \omega^*$  and  $\omega \ll \omega^*$ , respectively. Fitting Eq. (5) to the data in Fig. 3 leads to  $b_{\text{eff}} N_{\text{mp}} \approx 400$  independent of  $\sigma_0$ , suggesting that most dislocations would move either individually or within wall-like structures. However, while such a simple model results in the stress amplitude dependence observed in simulations, i.e.,  $A_{\text{hyst}}(\sigma_0) \sim \sigma_0^2$ , it obviously fails to reproduce correctly the nontrivial low-frequency  $\kappa$  exponents.

Thus it is necessary to go beyond such simplistic descriptions by considering ideas from critical phenomena, applied to a yielding transition [10,12]. It has been proposed that due to the long-range dislocation stress fields, this should be described by the mean-field depinning transition [15,16]. To test this idea within the present framework, we proceed to contrast our results with those obtained recently for a mean field elastic interface subject to ac driving [26]. There, the exponent of the low-frequency power law  $A_{\text{hyst}}(\omega) \sim \omega^\kappa$  describing the force-velocity (the latter being the order parameter of the depinning transition) hysteresis loop area has been shown to exhibit three regimes as a function of the applied force amplitude  $\sigma_0$ , with the exponent  $\kappa$  assuming the values  $\kappa \approx 0.67$  or  $0.75$  (for cusped and smooth disorder, respectively, Ref. [26]) for  $\sigma_0 \gg \sigma_c$ ,  $\kappa \approx 0.82$  for  $\sigma_0 \approx \sigma_c$  and  $\kappa \approx 1$  for  $\sigma_0 \ll \sigma_c$ .  $\sigma_c$  is the critical depinning force of the dc-driven system. Thus, in particular, our numerical results do not agree with the mean field depinning

scaling of the loop area for small force (stress) amplitudes, corresponding to the pinned (jammed) phase: the pinned phase of the mean field interface exhibits trivial dynamics, with the  $\kappa$  exponent coinciding with that of the naive oscillator model, whereas we find here a  $\kappa < 1$  for a wide range of stress amplitudes with  $\sigma_0 < \sigma_c$ . An additional difference is that for dislocations we observe only a single hysteresis loop [27], while for interface depinning models one typically observes a secondary loop with counterclockwise rotation direction for  $\sigma_0 \gg \sigma_c$  in the region  $\sigma > \sigma_c$  [13,26].

Consequently, our results reveal that various scaling features in the dynamic hysteresis of crystalline solids relate to the collective dynamics of dislocations. From the theoretical point of view the central observation is that unlike the pinned phase of conventional ac-driven mean field interfaces, the jammed phase of the dislocation system exhibits critical-like dynamics. In fact, the  $\kappa$  value we find for  $\sigma_0 < \sigma_c$  coincides with the mean field depinning result for  $\sigma_0 \approx \sigma_c$  ( $\kappa \approx 0.82$ ), suggesting that the system exhibits criticality in the entire region  $0 < \sigma_0 < \sigma_c$ . Similar observations have been made by Ispánovity *et al.* [25], who found that the dislocation system subject to a small constant stress exhibits glassy power-law relaxation up to a time scale limited only by the system size rather than the applied stress value. We think this is due to the dynamic nature of the effective disorder—the dislocations are subject and jam due to a random stress field rather than to quenched disorder absent here, but fundamental to conventional depinning models. Interesting extensions of the present study could include considering the effect of a nonlinear mobility law [9,28,29] (which might give rise to a dynamic transition [1,30]), or cyclic loading of alloys exhibiting the Portevin-Le Chatelier effect [31,32].

To conclude, the time-dependent loading of dislocations exhibits features that result from collective dynamics. This suggests that such signatures should be seen during the deformation of any material containing dislocations, and that they should also be looked for in the yielding of noncrystalline materials [33]. These findings call for new experimental (for instance in colloidal crystals [34]) and numerical studies (e.g., molecular dynamics simulations [35]) of cyclic dislocation dynamics, as well as novel theoretical ideas to properly describe dislocation jamming.

M.-C. Miguel, M. Zaiser and O. Vartia are thanked for discussions. This work has been supported by the Academy of Finland through a Postdoctoral Researcher's Project (LL, Project No. 139132) and via the Centers of Excellence Program (Project No. 251748).

- 
- [1] B. K. Chakrabarti and M. Acharyya, *Rev. Mod. Phys.* **71**, 847 (1999).  
 [2] J. P. Sethna, J. Sethna, K. Dahmen, S. Kartha, J. Krumhansl, B. Roberts, and J. Shore *Phys. Rev. Lett.*

- 70**, 3347 (1993); K. Dahmen and J.P. Sethna, *Phys. Rev. Lett.* **71**, 3222 (1993); D. Dhar, P. Shukla, and J.P. Sethna, *J. Phys. A* **30**, 5259 (1997).
- [3] T.A. Read, *Phys. Rev.* **58**, 371 (1940); A. Granato and K. Lücke, *J. Appl. Phys.* **27**, 789 (1956); *J. Appl. Phys.* **27**, 583 (1956); J.C. Bibello and M. Metzger, *J. Appl. Phys.* **38**, 849 (1967).
- [4] O.H. Schmitt, *J. Sci. Instrum.* **15**, 24 (1938); L. Chua, *IEEE Trans. Circuit Theory* **18**, 507 (1971).
- [5] J.R. Pomeroy, E.D. Sontag, and J.E. Ferrell Jr, *Nat. Cell Biol.* **5**, 346 (2003).
- [6] D. Williams, G. Phillips, and R. Sekuler, *Nature (London)* **324**, 253 (1986).
- [7] E.M. Chudnovsky, *Science* **274**, 938 (1996).
- [8] G. D'Anna, W. Benoit, and V.M. Vinokur, *J. Appl. Phys.* **82**, 5983 (1997).
- [9] M. Zaiser, *Adv. Phys.* **55**, 185 (2006).
- [10] M.-C. Miguel, A. Vespignani, M. Zaiser, and S. Zapperi, *Phys. Rev. Lett.* **89**, 165501 (2002).
- [11] M.-C. Miguel, L. Laurson, and M.J. Alava, *Eur. Phys. J. B* **64**, 443 (2008).
- [12] L. Laurson, M.-C. Miguel, and M.J. Alava, *Phys. Rev. Lett.* **105**, 015501 (2010).
- [13] A. Glatz, T. Nattermann, and V. Pokrovsky, *Phys. Rev. Lett.* **90**, 047201 (2003).
- [14] V. Metlushko, U. Welp, I. Aranson, S. Scheidl, V.M. Vinokur, G.W. Crabtree, K. Rogacki, and B. Dabrowski, *arXiv:cond-mat/9804121*.
- [15] M. Zaiser and P. Moretti, *J. Stat. Mech.* (2005) P08004.
- [16] K.A. Dahmen, Y. Ben-Zion, and J.T. Uhl, *Phys. Rev. Lett.* **102**, 175501 (2009).
- [17] M.-C. Miguel, A. Vespignani, A. Zapperi, J. Weiss, and J.R. Grasso, *Mater. Sci. Eng. A* **309–310**, 324 (2001).
- [18] E. van der Giessen and A. Needleman, *Model. Simul. Mater. Sci. Eng.* **3**, 689 (1995).
- [19] F. Csikor, C. Motz, D. Weygand, M. Zaiser, and S. Zapperi, *Science* **318**, 251 (2007).
- [20] M. Koslowski, R. LeSar, and R. Thomson, *Phys. Rev. Lett.* **93**, 125502 (2004).
- [21] O.U. Salman and L. Truskinovsky, *Phys. Rev. Lett.* **106**, 175503 (2011).
- [22] M.-Carmen Miguel, A. Vespignani, S. Zapperi, J. Weiss, and J.R. Grasso, *Nature (London)* **410**, 667 (2001).
- [23] J. Rosti, J. Koivisto, L. Laurson, and M.J. Alava, *Phys. Rev. Lett.* **105**, 100601 (2010).
- [24] L. Laurson, J. Rosti, J. Koivisto, A. Miksic, and M.J. Alava, *J. Stat. Mech.* (2011) P07002.
- [25] P.D. Ispánovity, I. Groma, G. Györgyi, P. Szabó, and W. Hoffelner, *Phys. Rev. Lett.* **107**, 085506 (2011).
- [26] F. Schütze and T. Nattermann, *Phys. Rev. B* **83**, 024412 (2011).
- [27] For very large  $\sigma_0$  and low  $\omega$  we see some double hysteresis, but in this regime the dislocation displacements are of the order of  $L$ , suggesting that periodic boundaries could have an effect.
- [28] E. Nadgorny, *Dislocations Dynamics and Mechanical Properties of Crystals* (Pergamon Press, Oxford, 1988).
- [29] W. Cai and V.V. Bulatov, *Mater. Sci. Eng. A* **387–389**, 277 (2004).
- [30] N. Fujiwara, T. Kobayashi, and H. Fujisaka, *Phys. Rev. E* **75**, 026202 (2007).
- [31] G. Ananthakrishna, *Phys. Rep.* **440**, 113 (2007).
- [32] M. Zaiser and P. Hähner, *Phys. Status Solidi B* **199**, 267 (1997).
- [33] A. Lemaitre and C. Caroli, *Phys. Rev. Lett.* **103**, 065501 (2009).
- [34] A. Pertsinidis and X.S. Ling, *New J. Phys.* **7**, 33 (2005).
- [35] P. Moretti, B. Cerruti, and M.-C. Miguel, *PLoS ONE* **6**, e20418 (2011).